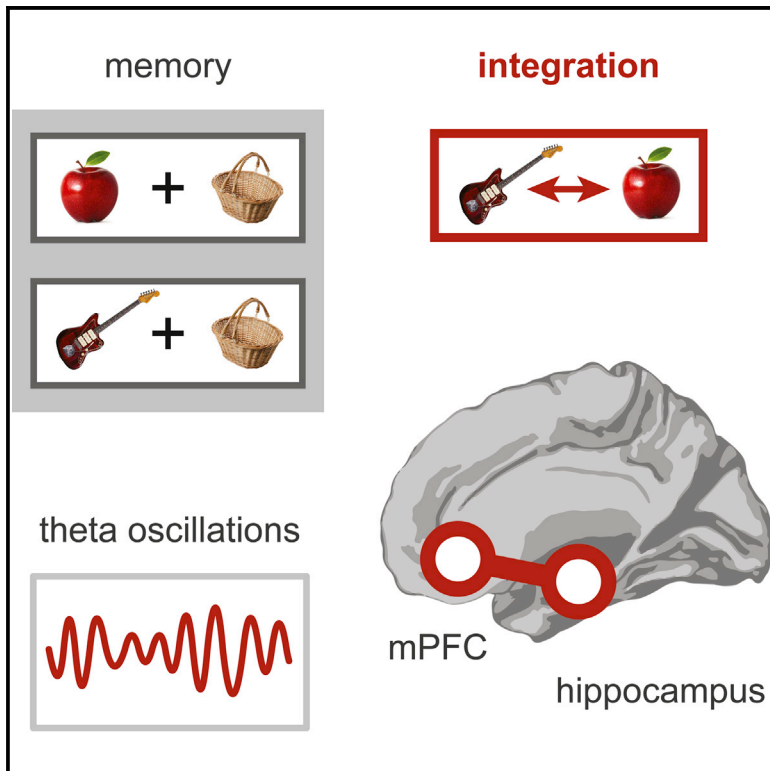


Hippocampal-Prefrontal Theta Oscillations Support Memory Integration

Graphical Abstract



Authors

Alexander R. Backus,
Jan-Mathijs Schoffelen,
Szabolcs Szebényi, Simon Hanslmayr,
Christian F. Doeller

Correspondence

a.backus@donders.ru.nl (A.R.B.),
c.doeller@donders.ru.nl (C.F.D.)

In Brief

Backus et al. use magnetoencephalography to show that amplitude and coupling strength of theta oscillations in hippocampal and medial prefrontal sources predict the successful integration of memories. Hereby, they reveal an important physiological mechanism underlying inferential reasoning, decision making, and knowledge acquisition.

Highlights

- We used deep-source MEG to study the physiological mechanism of memory integration
- Medial temporal lobe theta amplitude predicts successful integration of memories
- Memory integration involves increased hippocampal-mPFC theta coupling



Hippocampal-Prefrontal Theta Oscillations Support Memory Integration

Alexander R. Backus,^{1,*} Jan-Mathijs Schoffelen,^{1,2} Szabolcs Szebényi,^{1,3} Simon Hanslmayr,⁴ and Christian F. Doeller^{1,*}

¹Radboud University, Donders Institute for Brain, Cognition and Behaviour, 6525 Nijmegen, the Netherlands

²Max Planck Institute for Psycholinguistics, 6525 Nijmegen, the Netherlands

³University of Konstanz, 78464 Konstanz, Germany

⁴University of Birmingham, Birmingham B15 2TT, UK

*Correspondence: a.backus@donders.ru.nl (A.R.B.), c.doeller@donders.ru.nl (C.F.D.)

<http://dx.doi.org/10.1016/j.cub.2015.12.048>

SUMMARY

Integration of separate memories forms the basis of inferential reasoning—an essential cognitive process that enables complex behavior. Considerable evidence suggests that both hippocampus and medial prefrontal cortex (mPFC) play a crucial role in memory integration. Although previous studies indicate that theta oscillations facilitate memory processes, the electrophysiological mechanisms underlying memory integration remain elusive. To bridge this gap, we recorded magnetoencephalography data while participants performed an inference task and employed novel source reconstruction techniques to estimate oscillatory signals from the hippocampus. We found that hippocampal theta power during encoding predicts subsequent memory integration. Moreover, we observed increased theta coherence between hippocampus and mPFC. Our results suggest that integrated memory representations arise through hippocampal theta oscillations, possibly reflecting dynamic switching between encoding and retrieval states, and facilitating communication with mPFC. These findings have important implications for our understanding of memory-based decision making and knowledge acquisition.

INTRODUCTION

During everyday life, we continuously bind new information into coherent episodic memories [1]. Although these memories are inherently separated in time, we have the remarkable ability to link and recombine episodes with overlapping elements [2–4]. Integration of multiple events into a new memory forms the basis of inferential reasoning [1], regularity learning [5], and decision making and ultimately the formation of our knowledge base [4].

Evidence from animal lesion studies [6] and human neuroimaging [3, 7–12] has demonstrated that the medial prefrontal cortex (mPFC) and hippocampus [2] are the two key regions implicated in memory integration. Interestingly, human func-

tional MRI (fMRI) studies have revealed increased functional connectivity between these two key nodes during memory encoding and retrieval, including integrating information across events [3]. However, due to the low temporal resolution of fMRI, the electrophysiological mechanisms underlying this crosstalk by which hippocampus and mPFC are able to retrieve, exchange, integrate, and re-encode multiple memories on a millisecond timescale remain poorly understood.

Rhythmic theta band activity in the hippocampus (traditionally 4–8 Hz in humans, 6–10 Hz in rodents), which is strongly associated with place cell activity [13], has been implicated in memory formation by intracranial recording studies [14], although human studies commonly report effects at the lower end of the traditional theta band [15, 16]. More recently, these findings have been corroborated by studies using magnetoencephalography (MEG) [17–20], supported by modeling and invasive recording efforts that confirm the feasibility of reconstructing hippocampal theta oscillations from MEG sensor data [21].

In addition, interregional coupling of theta oscillations in hippocampus and mPFC has been observed during memory encoding, retrieval, and decision making in animals [22, 23] and humans, using intracranial recordings [24] and MEG [19]. Such oscillatory coupling between distant regions has been put forward as an electrophysiological mechanism for information transfer [25]. Taken together, these findings suggest that theta oscillations might be involved in orchestrating the integration of memories. Theoretical models and recent neuroimaging evidence suggest that memory integration is achieved through retrieval-mediated learning [3, 8]. Since theta oscillations have been posited to gate information flow during alternating encoding and retrieval states [26], we hypothesize that rhythmic theta band activity plays an important role during memory integration, where an existing memory is retrieved and re-encoded together with a new memory.

In sum, while mPFC and hippocampus appear to play a crucial role in integrating multiple memories, the underlying electrophysiological mechanism remains unclear. Synchronized theta oscillations are likely to provide such a mechanism, but their region-specific involvement in human memory integration remains elusive. To resolve this outstanding issue, we used MEG to record whole-brain oscillatory activity of participants performing a classic associative inference paradigm [8]. We leveraged novel source reconstruction methods to measure hippocampal theta oscillations and employed coherence analysis to investigate oscillatory coupling with mPFC. Critically, we aimed to pinpoint

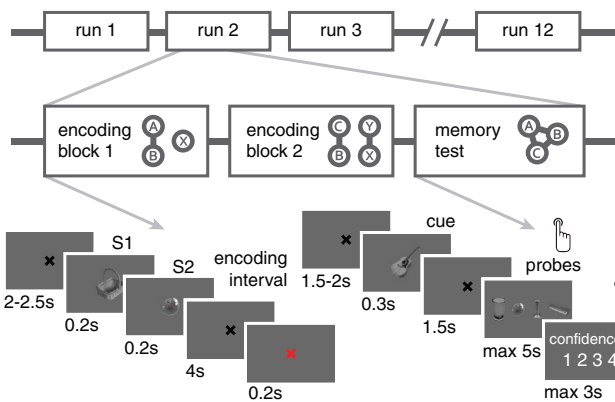


Figure 1. Experimental Procedure and Trial Structure of the Memory Integration Task

Top: in 12 cycles, participants learned dyad (YX) and triad (ABC) associations between gray-scale pictures of objects during two separate encoding blocks. Subsequently, memory was probed for both directly associated objects (AB, CB, YX) and inferred associations (AC). Bottom: each encoding trial comprised serial presentation of two objects (S1 and S2: first and second stimulus), followed by a dedicated encoding interval. A red fixation cross indicated a short blink phase and the upcoming new trial. Test trials commenced with a cue, a retrieval phase, a forced-choice response phase with four alternatives and concluded with a memory confidence rating.

electrophysiological markers during encoding of novel information that are predictive of successful integration with an existing memory.

RESULTS

Participants performed an associative inference task [9] modified for MEG, in which pairs of to-be-associated object stimuli were briefly presented in sequence (see [Experimental Procedures](#) for details). Pairs comprised so-called premise associations (AB and CB pairs) and a control association (YX pair). Crucially, participants were asked to subsequently infer an indirect, unseen link (AC association) between the overlapping AB and CB pairs (Figure 1) and thus encode a collection of triad (ABC) and dyad (YX) memories. Following encoding, we tested the participant's memory for all associations. On average, participants correctly remembered 79.8% (SEM = 2.8%) of AB pairs, 75.0% (SEM = 3.7%) of YX pairs, 69.0% (SEM = 3.8%) of CB pairs, and 62.3% (SEM = 3.9%) of the crucial inferred AC associations (Figure 2A). We observed a clear pattern across different association types: the second premise pairs (CB) were remembered significantly worse than the initial AB premise pairs ($T_{26} = 8.13$, $p = 1^{-5}$ Bonferroni-corrected [corr]) and control YX pairs ($T_{26} = 3.81$, $p = 0.006$, corr). In turn, performance on directly associated objects, including the CB pairs, significantly surpassed inferred AC associations ($T_{26} = 4.75$, $p = 0.0004$, corr). Next, we excluded seven participants from subsequent MEG analyses, who were unable to reach the performance criterion on AC association tests (see [Experimental Procedures](#) for details). Based on final performance, we categorized each individual triad into eight possible categories, ranging from “no links remembered” to “all links remembered” (Figure 2B). Through behavioral piloting, we had adjusted task difficulty to obtain

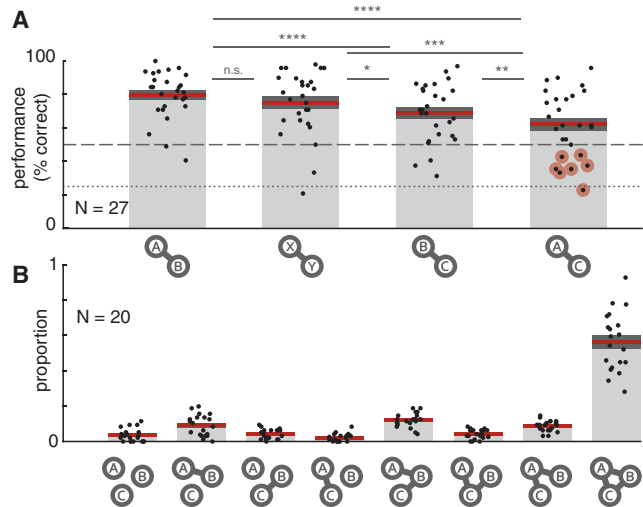


Figure 2. Behavioral Performance

(A) Across different association types, performance for premise pairs was better than for inferred pairs. Schematics below bars depict different conditions (e.g., AB nodes with an edge symbolize AB pair correct). Red line: mean, darker shaded area: SEM, dotted line: accuracy chance level, dashed line: exclusion criterion, red-circled dots: excluded participants, * $p < 0.01$, ** $p < 0.001$, *** $p < 0.0001$, **** $p < 0.00001$.

(B) Proportion of triad associations in each fine-grained performance category (see schematic below bars). Each dot represents data from a single participant (A and B).

roughly half of the triads in the “all links remembered” category (mean = 56.5%, SEM = 3.8%).

To test our primary hypothesis that hippocampal theta oscillations are involved in memory integration, we applied a “subsequent integration contrast” (Figure 3A). Here, we compared brain activity during CB encoding trials where the AC association was later successfully integrated, with a subset of encoding trials where the CB premise or XY association was remembered, but, crucially, no indirect AC link was inferred. By including brain activity related to direct associative encoding of the premise pair in the non-integration subset, we aimed to isolate processes contributing to memory integration. After removing effects due to eye-movements (see [Supplemental Experimental Procedures](#) for control analysis) and other artifacts from the signal, we pursued a novel, advanced region of interest (ROI) source reconstruction method to estimate theta power from left and right hippocampus. In particular, we applied leadfield reduction based on anatomical priors (see [Experimental Procedures](#) for details and Figure 5 for a graphical depiction) where we took into account the structure of the hippocampus. Initially, we targeted a broad frequency range of theta oscillations spanning 3–7 Hz—a slightly lower frequency than the traditional theta band, based on recent reports [15, 16]. Using a sliding time window, we obtained the time course of theta power and converted the values to normalized difference scores (T-statistics) for the subsequent integration contrast, separately for left and right hippocampus. Since previous electrophysiological work has demonstrated that memory retrieval and encoding occurs rapidly [27], we focused our initial statistical test on the first two seconds of the encoding interval. We found a significant

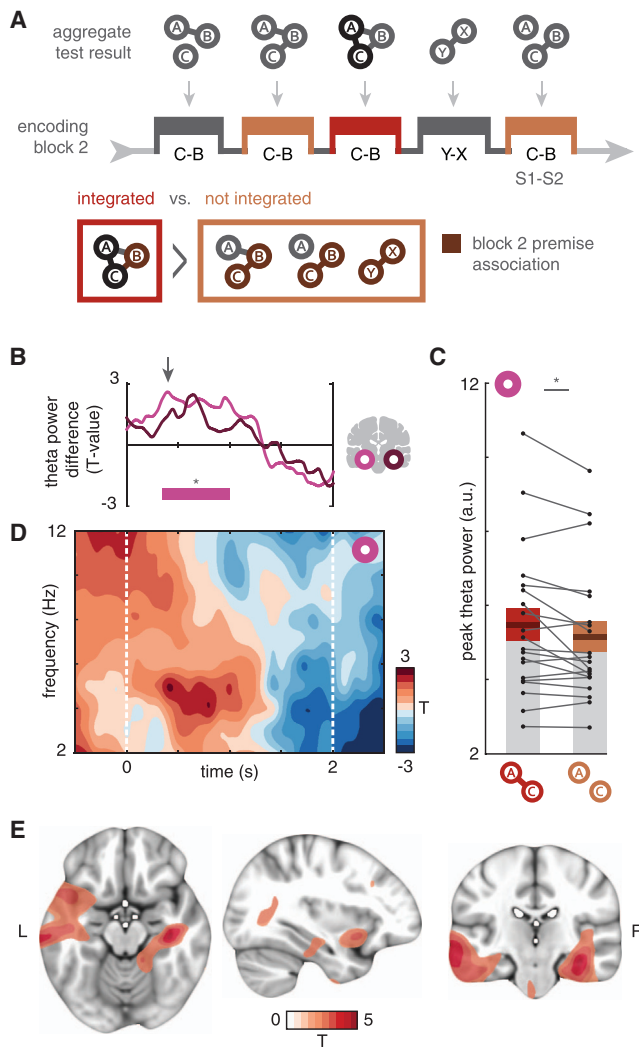


Figure 3. Hippocampal Theta Power Predicts Successful Memory Integration

(A) Subsequent integration contrast: each triad or dyad was categorized according to its aggregate memory test result (top row). This categorization was used to assign the corresponding encoding trial from the second block to the integration (red) or non-integration (orange) condition. The middle row shows a stream of five encoding trials, colored according to their condition assignment. Brain activity during integration trials was contrasted with non-integration trials, controlling for direct encoding of the premise pair (dark brown link).

(B) Normalized theta power (3–7 Hz) difference scores (T-statistics) over time for left (light purple) and right hippocampus (dark purple) for the subsequent integration contrast. Time-axis from (D), where $t = 0$ marks the start of the encoding interval. Horizontal bar indicates significant theta power increase in left hippocampus from 300 to 1,000 ms into the encoding interval. * $p < 0.05$ cluster-corrected.

(C) Peak statistics for each separate condition, where each dot represents one participant. Colored line, mean; lighter shaded area, SEM.

(D) Full time-frequency representation of left hippocampus. Red indicates stronger theta power during successful integration, while blue denotes stronger theta power during non-integration trials. White dotted lines show the statistical window-of-interest used in (A). In order to display all data, we applied no threshold to the T-values.

(E) Whole-brain spatial distribution of theta power 400 ms into the encoding interval. Slices (x, y, z = [-33, -22, -16]) were selected in order to visualize effects in both left and right hippocampus. Maps thresholded at cluster-threshold value $p < 0.01$ for display purposes.

difference in theta amplitude ($p = 0.04$ cluster-corrected), where power in the left hippocampus was increased from 350 to 1,000 ms following stimulus offset in successful integration trials, compared to non-integration trials (Figure 3B). Overall, right hippocampus showed a similar pattern of theta power differences over time, albeit non-significant (power increase: $p > 0.31$ cluster-corrected). The left hippocampal theta increase peaked at 400 ms into the encoding interval (Figure 3C, $T_{19} = 2.58$, $p = 0.007$, Bayes Factor [BF₁₀] = 6.1, see Experimental Procedures for details). Note that due to the applied estimation procedure, this effect contains data from a 1-s time window spanning -100 to 900 ms.

In a next step, we performed a frequency-resolved follow-up analysis to display the spectrotemporal specificity of the described early theta difference (Figure 3D; see Figure S1 for right hippocampus). In addition, we corroborated results from left hippocampus with an alternative source reconstruction algorithm (Figure S2) and sensor level data showing a similar pattern in temporal sensors (Figure S3; see Figure S4 for an exploratory analysis of other frequency bands). Finally, we estimated theta power of a whole-brain source grid at the peak time window and computed difference scores with the subsequent integration contrast (Figure 3E). As expected, we observed a significant difference between conditions ($p = 0.01$, whole-brain cluster-corrected) with a spatially specific cluster in the left hemisphere (peak of cluster in middle temporal gyrus, Brodmann area 21; x, y, z = [-76, -24, -16], $T_{19} = 3.92$, extending into hippocampus). In addition, we observed a cluster in the right hippocampus ($p = 0.03$ whole-brain cluster-corrected; peak of cluster in superior temporal gyrus, Brodmann area 22; x, y, z = [44, -16, -8] $T_{19} = 4.07$, including right hippocampus). We observed no other significant theta power increases in the brain ($p > 0.44$ whole-brain cluster-corrected, see Table S1 for list of brain regions thresholded at $p < 0.01$ uncorrected).

In a second analysis, we investigated functional coupling between the left hippocampus and mPFC at the peak time window of the theta power subsequent memory integration effect. To this end, we performed a seed-based functional connectivity analysis, in which we computed coherence across trials between the left hippocampal ROI signal and the whole-brain grid sources (Figures 4A and 4B). We then searched for coupling effects inside an anatomically defined area comprising mPFC [10]. We observed a significant difference in coupling ($p = 0.03$ search-volume cluster-corrected), with a spatially selective cluster in mPFC where theta oscillations were more strongly coupled with left hippocampal theta when integration was successful, compared to non-integration trials (Figures 4B and 4C, peak: x, y, z = [-4, 40, -8]). The cluster mainly covers left mPFC and included parts of Brodmann areas 10, 11, and 25, with a local peak coherence in the orbital part of the left middle frontal gyrus ($T_{19} = 2.97$, $p = 0.004$, BF₁₀ = 12). Markedly, we found that the peak coherence voxel did not show a significant increase in theta power ($T_{19} = -0.92$, $p = 0.81$), with evidence suggesting that theta power levels did not differ across conditions (BF₁₀ = 0.13, support for null-hypothesis: BF₀₁ = 7.5). Therefore, the observed coherence increase is unlikely to constitute a side effect of a potential overall signal amplitude increase. In addition, we observed a similar pattern of results when we used phase-locking values, a coupling measure that is less sensitive to

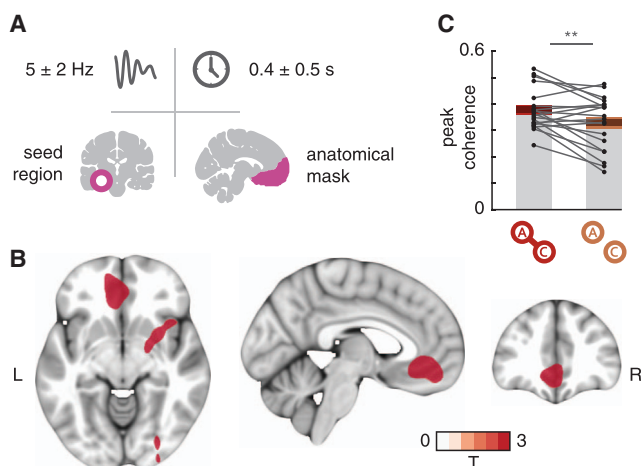


Figure 4. Hippocampal-Prefrontal Coupling Signals Successful Memory Integration

(A) Seed-based theta coupling analysis logic. Time-frequency window of the peak theta power effect was used to compute theta coherence of left hippocampal seed region to the rest of the brain, focusing on anatomically delineated mPFC (see schematic of mask).

(B) Brain regions showing increased coherence with left hippocampus in the subsequent integration contrast. Slices centered on the coherence peak in mPFC. Maps were thresholded at cluster-threshold $p < 0.01$ for display purposes.

(C) Peak statistics for both conditions separately, where each dot represents the peak coherence of left hippocampus to mPFC of one participant. Note that although raw coherence metrics are displayed here, debiased Z-transformed measures were used for the significance test. ** $p < 0.005$.

co-variation in power between regions (Figure S5A). In both conditions, phase delays between left hippocampus and the mPFC peak voxel did not cluster around zero (Figure S5B), suggesting that the observed phase coupling effects are not due to spatial leakage of activity (see Supplemental Experimental Procedures for details). There were no other significant theta coherence increases in the brain ($p > 0.08$ whole-brain cluster-corrected, see Table S2 for list of brain regions thresholded at $p < 0.01$ uncorrected).

DISCUSSION

In this study, we have demonstrated the involvement of hippocampal and prefrontal theta oscillations in memory integration in humans. By leveraging the high temporal resolution of MEG, we showed that theta signals in the medial temporal lobe increase in amplitude when a new memory is successfully incorporated into an existing mnemonic representation.

Rhythmic activity in the theta frequency band is the most prominent type of activity signaling the online state of the hippocampus and surrounding medial temporal brain regions [28]. Individual cell firing is phase-locked to theta waves, generating phase-coding and neuronal population sequences [13]. Moreover, the alternating phases of theta are implicated in rapid switching between inputs and outputs of the hippocampus [26, 29]. This input-output gating has been put forward as a mechanism to segregate encoding and retrieval states and prevent potential interference [26]. A large body of evi-

dence directly links theta to memory function: on the cellular level, rhythmic excitability modulation by theta is essential for long-term synaptic potentiation [30]. On the population level, theta amplitude tends to markedly increase when novel information is encoded and stored information retrieved from memory, for instance, during spatial navigation [19] and decision making [18]. Moreover, global differences in theta oscillations both during and preceding encoding have been linked to memory performance [31–33]. Interestingly, some studies report increases [31, 33] while others report decreases [32] in theta power during successful memory encoding, leaving the precise contribution of theta to memory unresolved. The behavioral benefits or detrimental effects of enhanced theta oscillations during encoding might highly depend on differences in encoding strategies and memory tests across subsequent memory studies [34]. In our data, we also observed a theta decrease in the later phase of the encoding window, which could be potentially due to conflict processing in the non-integration condition [35] or enhanced information processing in the integration condition via oscillatory desynchronization [34]. However, with our hypothesis-based approach, we investigate a very specific role for increases in theta oscillations during the integration of prior memories with new information, going beyond traditional subsequent memory studies.

Previous electrophysiological work has demonstrated that a retrieval cue can lead to reactivation of a memory very rapidly, within 500 ms [27]. In line with these reports, we showed a similar time course during memory integration. The significant increase in theta oscillations 350 ms after stimulus presentation suggests that encoding of the inferred association (AC) immediately follows the reactivation of the premise association (AB). This observation accords with the retrieval-mediated learning hypothesis [3]. Taken together, our findings support the notion of theta oscillations as the key operating mechanism of the hippocampus for information processing. In particular, during retrieval-mediated learning of an integrated memory, hippocampal theta oscillations might subserve segregation of the necessary retrieval and encoding processes [26].

In addition to a hippocampal theta amplitude increase, we showed that enhanced theta coupling between hippocampus and mPFC predicts successful memory integration. Our findings are consistent with previous observations of hippocampal-prefrontal interactions during spatial navigation [19], decision making [18], and other memory tasks [36]. In particular, we corroborate previous fMRI studies showing the importance of hippocampal-prefrontal crosstalk for memory integration [3]. However, here, we go beyond these reports by elucidating the electrophysiological mechanism behind this interaction: theta oscillatory coupling. In general, many neocortical regions synchronize with hippocampal theta oscillations [37]. However, here, we demonstrated that specifically the mPFC exhibits increased coupling during memory integration. Thereby, we provide evidence for theta-mediated functional interactions between these two key brain regions. Functional communication between hippocampus and mPFC during memory integration is supported by strong reciprocal anatomical connections. The anterior hippocampus has monosynaptic projections to mPFC [38]. In turn, the mPFC projects back to the hippocampus via the entorhinal cortex, in addition to a subcortical pathway with

a thalamic relay [39]. These projections from mPFC to hippocampus have recently been shown to play a crucial role in retrieving sparse hippocampal memory representations [40] and are therefore important for memory integration through retrieval-mediated learning. In addition, theta peak frequency has been found to correlate with structural connectivity between hippocampus and mPFC, suggesting that theta oscillations are mediating interregional communication [41]. But how might theta oscillatory coupling facilitate hippocampal-prefrontal neuronal interactions in service of memory integration? Oscillatory coupling has been put forward as a mechanism for long-range information exchange between brain regions [25]. By synchronizing the excitable phases of neuronal populations in distant brain regions, a window for effective communication is established. Potentially, the hippocampus imposes phase-locking of neurons in the mPFC, enforcing that only task-relevant inputs are selected and amplified in each subsequent theta cycle. Alternatively, mPFC might bias reconfiguration of hippocampal cell assemblies by entraining theta oscillations. Theta-dependent spatially selective hippocampal place cells are known to remap when encoding similar environments [29]. One could speculate that when encoding a new but similar memory, cells coding for the already existing memory need to be reconfigured (i.e., remapped) for successful integration. This reconfiguration process may be facilitated by resetting the phase of ongoing hippocampal theta oscillations [42], allowing the encoding of a novel combined memory. In addition, phase coupling between hippocampus and mPFC may also enable exchange of information represented by phase-coded neuronal population sequences [43]. Taken together, our findings are in line with the idea that theta coupling provides the electrophysiological mechanism through which these key regions interact and integrate novel information with an overlapping existing memory.

Hippocampus and the mPFC have been put forward as core nodes of the neural circuit for memory integration and generalization [2, 39]. But do the two regions have specialized roles during memory integration? Computational models [44] propose that the hippocampus encodes and retrieves specific associations, whereas the cortex extracts common features across events. Accordingly, the hippocampus separates neural patterns associated with distinct events, whereas the mPFC might combine patterns of overlapping events [45]. Evidence from human neuroimaging studies supports the pattern-separation function of the hippocampus, by demonstrating its involvement in various episodic memory tasks [8]. Likewise, the mPFC has been implicated in generating adaptive responses to current events based on past experience [46]. By accumulating contextual information of overlapping episodic memories, the mPFC constructs mnemonic schemas or networks, which represent prior knowledge to guide decision making [2, 47]. However, it remains unclear whether the division of labor between hippocampus and mPFC is strictly dichotomous, since both pattern completion and pattern separation are known to take place in the hippocampus. Hippocampal cells express firing patterns for overlapping contexts, suggesting the hippocampus itself is also involved in generalization across episodes [1]. In addition, recent neuroimaging findings corroborate the idea that the hippocampus simultaneously performs episode segregation and integration [11]. Nonetheless, our results indicate that both the

hippocampus and the mPFC play an important role during memory integration, potentially via retrieval-mediated learning and pattern completion of overlapping memories.

Memory integration is the key process underlying regularity extraction and generalization across similar events and situations. However, a tradeoff between memory specificity and generalization is vital to prevent maladaptive overgeneralization of memories. Here, we provide evidence for a crucial role of hippocampal-prefrontal theta coupling in memory generalization. Further investigations of this electrophysiological signature might improve our understanding of psychopathologies linked to overgeneralization, such as posttraumatic stress disorder and depression [39]. Moreover, our findings might guide future attempts to bias memory integration by manipulating or entraining region-specific theta oscillations. Facilitating or impeding the integration of specific pieces of information might help us to potentially accelerate learning and enhance knowledge acquisition.

Taken together, our findings highlight the involvement of hippocampus and mPFC in memory integration. Theta oscillations orchestrate the integration of memories by engaging the hippocampus and facilitating communication between hippocampus and mPFC. These mechanisms constitute the crucial first step in the formation of relational memory networks, enabling us to assimilate information and ultimately expand our knowledge base.

EXPERIMENTAL PROCEDURES

Data Acquisition

Participants performed an adapted version of the associative inference task used by Zeithamova and Preston [9] (Figure 1) while MEG data were recorded (see [Supplemental Experimental Procedures](#) for details). Experimental procedures were reviewed and approved by the local ethical review committee (CMO committee on Research Involving Humans, region Arnhem-Nijmegen, the Netherlands). We randomly paired object stimuli to create 96 triad associations (ABC) and 48 dyads (YX). Participants were exposed to premise associations (AB and CB pairs) and control associations (YX pairs), followed by a memory test in 12 independent cycles. Crucially, the AC association of a triad was never directly encoded, although memory for this inferred association was tested. Each cycle comprised two separate encoding blocks, followed by a test block, allowing us to assess memory performance. After an initial analysis of behavioral data (Figure 2A; see [Supplemental Experimental Procedures](#) for details), seven participants were excluded based on their low inference performance level (criterion at double chance level: at least 50% correct, to ensure sufficient trials per condition). The MEG data of 20 high-performing participants in total were preprocessed (see [Supplemental Experimental Procedures](#) for details) and further analyzed.

Subsequent Integration Contrast

To isolate the neural oscillatory signatures of memory integration, we contrasted encoding-related activity during fully successful integration trials in block 2 (AB, CB, and AC correct) with non-integration trials (AB and CB correct, CB correct, and YX correct). Crucially, a premise or direct association was nonetheless successfully encoded during all non-integration trials (Figure 3A). Thereby, we isolated activity related to successful AC inference and subsequent integration into the ABC triad. To prevent bias in source activity estimation, we equalized the number of trials in each condition set to match the smaller subset size, by selecting a random subsample once. Across participants, on average 41 trials per condition entered the final analysis (range: 25–56 trials, SD: eight trials).

Source Reconstruction

With a strong a priori hypothesis on the hippocampus—a well-defined anatomical brain region—we employed an ROI source reconstruction

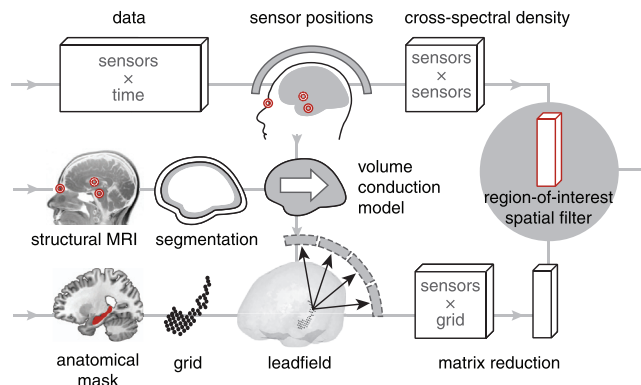


Figure 5. Hippocampus-Based MEG Source Reconstruction Procedure

Based on participant-specific anatomy, we constructed a realistic volume conduction model (middle). In parallel, we created a high-resolution grid spanning a specific anatomical ROI, aligned to a common template space (bottom). Using the volume model and sensor position information, we computed a leadfield for each grid point and performed feature reduction on the resulting matrix (i.e., forward solution). A beamformer algorithm was used to compute a spatial filter, with the reduced leadfield matrix and data covariance structure (cross-spectral density) as input (i.e., inverse solution).

technique (Figure 5), where we created leadfields based on anatomical priors [48]. Hereby, we aimed to compute one leadfield generated by the entire hippocampus, in contrast to the more traditional approach where one independently reconstructs a collection of point sources and averages afterward. First, we spawned a regular 5-mm grid covering all voxels inside the “Hippocampus_L” and “Hippocampus_R” anatomical masks from the Automated Anatomical Labeling atlas, with 2 mm smoothing, in Montreal Neurological Institute (MNI) space. Next, for each participant, we normalized the MNI grid based on the participant’s brain morphology taken from an individual structural MRI (see Supplemental Experimental Procedures for details), so that each grid point would cover roughly the same anatomical location across participants. The brain tissue segment from the structural MRI was used to construct a volume conduction model, based on the single-shell method [49]. Using this model, we computed how a dipolar source at each grid point would project to the sensors, yielding a forward model in the form of a sensors-by-grid point leadfield matrix (Figure 5, bottom). In a next step, we used singular value decomposition to reduce the number of columns in the leadfield matrix, by selecting the top left-singular vectors explaining at least 95% of the variance. Each hippocampal ROI leadfield matrix comprised six to eight spatial components. For the subsequent spatial filter estimation, we took the equalized sets of trials in each condition and combined them into one dataset. By using a balanced common filter approach, we aimed to prevent a potential bias toward one of the conditions. Next, we applied a Fourier transformation to the data from the full 0- to 4,000-ms encoding window, using multitapering. 15 tapers from discrete prolate spheroidal sequences (DPSS) were used for spatial filter estimation with 2 Hz spectral smoothing. From the complex-valued Fourier coefficients, we computed the cross-spectrum (Figure 5, top) for our frequency bands-of-interest (see next section for specifications). We used the entire encoding window—a continuous interval without visual stimulation—to improve estimation of the cross-spectrum. Next, we employed a Dynamic Imaging of Coherent Sources (DICS) beamformer [50] to estimate oscillatory activity at the source level. The cross-spectrum was regularized prior to matrix inversion by loading the diagonal of the matrix with 5% of the average sensor power. We used the DICS beamformer to fit a dipole for each of the spatial components and obtained a spatial filter for each ROI (Figure 5, right). Subsequently, we projected Fourier-transformed single trial sensor data through the spatial filter to reconstruct the source components comprising each ROI. To obtain theta power of the ROI as a whole, we combined information from each source component by taking the trace of the source cross-spectral density matrix. For the whole-brain source reconstruction

analysis, we employed a standard 8-mm MNI grid. Here, we projected the three resulting dipole moments (x, y, and z direction) by taking the principal eigenvector of the real part of the cross-spectral density matrix (kept constant across trials). For the connectivity analysis, this projection method was also applied to obtain complex-valued Fourier coefficients for the left hippocampal ROI.

Theta Power Analysis

In an initial step, we targeted the 3- to 7-Hz frequency band by using 2 Hz spectral smoothing centered on 5 Hz, with a 1,000-ms sliding time window in steps of 50 ms spanning a time window-of-interest from 0 to 2,000 ms. Spectral data from the three resulting orthogonal Slepian tapers were projected through precomputed spatial filters for left and right hippocampus. We quantified differences between the integration and non-integration conditions by computing T-statistics of this contrast across participants. We tested for exchangeability across conditions based on the resulting variance-normalized theta difference time course for left and right hippocampus together, using a one-tailed, paired t test (cluster-based permutation) with 100,000 permutations (time point cluster-inclusion criterion: $p < 0.05$ nonparametric on individual time point level, cluster statistic: summed T-values). For display purposes, the theta difference time course was smoothed using shape-preserving piecewise cubic interpolation. Power values from the peak time point showing the strongest normalized difference were extracted for each individual condition, and the associated significance value of the difference was obtained using a one-tailed nonparametric paired t test with 100,000 permutations. In addition, Bayes factors were computed using the standardized implementation of the Bayesian paired samples t test in the JASP software package (v.0.7.1.12, <https://jasp-stats.org/>) to indicate how much more likely our hypothesis (i.e., more theta power in the successful integration condition) is than the null hypothesis (i.e., no difference). For the frequency-resolved follow-up analysis, we used a 1,000-ms sliding time window to cover the -500- to 2,500-ms interval with steps of 100 ms. We explored frequencies from 2 to 12 Hz in steps of 1 Hz, with 2 Hz spectral smoothing. We applied the subsequent integration contrast to obtain T-value difference maps. The resulting time-frequency representations from left and right hippocampus were interpolated for display purposes. To obtain a whole-brain spatial distribution of the subsequent integration effect, we computed source activity in the full 8-mm grid at the peak time point. We used a whole-brain cluster-based permutation paired t test (10,000 permutations, cluster statistic: summed T-values). The voxel cluster inclusion criterion was set to $p < 0.01$ (nonparametric on individual voxel level) in order to obtain separate statistics for left and right hemisphere clusters. For display purposes, we interpolated the resulting maps to the MNI152 anatomical template with a resolution of 0.5 mm and thresholded the maps at the cluster inclusion threshold value. All brain images are displayed according to neurological convention.

Coupling Analysis

For the seed-based functional connectivity analysis, we collected the complex Fourier output for both the left hippocampal ROI and the whole-brain grid at the peak time point revealed by the power analysis (1-s time window from -100 to 900 ms, 5 Hz center frequency with 2 Hz spectral smoothing). Next, we computed across-trial coherence between the left hippocampus and each individual grid point, resulting in a whole-brain coherence map for each participant. After Fisher-Z transformation of the coherence measure, we debiased the data by dividing by the square root of the summed inverse degrees of freedom in each condition. The resulting debiased maps were subjected to a one-tailed cluster-based permutation paired t test across participants (10,000 permutations, cluster statistic: summed T-values) with a voxel cluster inclusion criterion of $p < 0.01$ (nonparametric on individual voxel level). Since we had a strong a priori hypothesis about the approximate brain region communicating with hippocampus, we restricted the statistical analysis to the anatomically delineated mPFC. We used a hand-drawn mPFC mask from a previous fMRI memory integration study, which encompassed all cytoarchitectonic subdivisions of mPFC associated with the limbic system [10]. We did not employ the ROI source reconstruction technique for mPFC due to its extent and functional subparcellation but used the regular point source grid for the connectivity analysis instead. The mPFC mask in MNI space was

interpolated to this 8-mm grid space using nearest-neighbor interpolation. Post hoc statistics on the peak coherence voxel were obtained using a one-tailed, nonparametric, paired t test with 100,000 permutations.

SUPPLEMENTAL INFORMATION

Supplemental Information includes Supplemental Experimental Procedures, five figures, and two tables and can be found with this article online at <http://dx.doi.org/10.1016/j.cub.2015.12.048>.

AUTHOR CONTRIBUTIONS

C.F.D. conceived the research. A.R.B., S.S., S.H., and C.F.D. designed the research. A.R.B. and S.S. performed the research. J.-M.S. contributed new analytic tools. A.R.B., S.S., and J.-M.S. analyzed data. A.R.B. and C.F.D. wrote the manuscript. All authors discussed the results and contributed to the manuscript.

ACKNOWLEDGMENTS

This work was supported by the European Research Council (ERC-StG 261177 to C.F.D. and ERC-CoG 647954 to S.H.), the Netherlands Organisation for Scientific Research (NWO-Vidi 452-12-009 to C.F.D. and NWO-Vidi 864-14-011 to J.-M.S.), and a grant from the German Research Foundation (HA 5622/1-1 to S.H.). The authors would like to thank S. Whitmarsh for help with graphics for Figure 5, J.L.S. Bellmund and S.E. Bosch for insightful discussions, M.L. Schlichting for sharing the mPFC mask, and T. Staudigl and C. Barry for useful comments on the manuscript.

Received: November 18, 2015

Revised: December 9, 2015

Accepted: December 9, 2015

Published: January 28, 2016

REFERENCES

- Eichenbaum, H., Dudchenko, P., Wood, E., Shapiro, M., and Tanila, H. (1999). The hippocampus, memory, and place cells: is it spatial memory or a memory space? *Neuron* 23, 209–226.
- Preston, A.R., and Eichenbaum, H. (2013). Interplay of hippocampus and prefrontal cortex in memory. *Curr. Biol.* 23, R764–R773.
- Zeithamova, D., Dominick, A.L., and Preston, A.R. (2012). Hippocampal and ventral medial prefrontal activation during retrieval-mediated learning supports novel inference. *Neuron* 75, 168–179.
- Kumaran, D., Summerfield, J.J., Hassabis, D., and Maguire, E.A. (2009). Tracking the emergence of conceptual knowledge during human decision making. *Neuron* 63, 889–901.
- Doeller, C.F., Opitz, B., Krick, C.M., Mecklinger, A., and Reith, W. (2005). Prefrontal-hippocampal dynamics involved in learning regularities across episodes. *Cereb. Cortex* 15, 1123–1133.
- Bunsey, M., and Eichenbaum, H. (1996). Conservation of hippocampal memory function in rats and humans. *Nature* 379, 255–257.
- Horner, A.J., Bisby, J.A., Bush, D., Lin, W.J., and Burgess, N. (2015). Evidence for holistic episodic recollection via hippocampal pattern completion. *Nat. Commun.* 6, 7462.
- Shohamy, D., and Wagner, A.D. (2008). Integrating memories in the human brain: hippocampal-midbrain encoding of overlapping events. *Neuron* 60, 378–389.
- Zeithamova, D., and Preston, A.R. (2010). Flexible memories: differential roles for medial temporal lobe and prefrontal cortex in cross-episode binding. *J. Neurosci.* 30, 14676–14684.
- Schlichting, M.L., Mumford, J.A., and Preston, A.R. (2015). Learning-related representational changes reveal dissociable integration and separation signatures in the hippocampus and prefrontal cortex. *Nat. Commun.* 6, 8151.
- Milivojevic, B., Vicente-Grabovetsky, A., and Doeller, C.F. (2015). Insight reconfigures hippocampal-prefrontal memories. *Curr. Biol.* 25, 821–830.
- Collin, S.H.P., Milivojevic, B., and Doeller, C.F. (2015). Memory hierarchies map onto the hippocampal long axis in humans. *Nat. Neurosci.* 18, 1562–1564.
- O'Keefe, J., and Recce, M.L. (1993). Phase relationship between hippocampal place units and the EEG theta rhythm. *Hippocampus* 3, 317–330.
- Lega, B.C., Jacobs, J., and Kahana, M. (2012). Human hippocampal theta oscillations and the formation of episodic memories. *Hippocampus* 22, 748–761.
- Jacobs, J. (2014). Hippocampal theta oscillations are slower in humans than in rodents: implications for models of spatial navigation and memory. *Philos. Trans. R. Soc. Lond. B Biol. Sci.* 369, 20130304.
- Watrous, A.J., Tandon, N., Conner, C.R., Pieters, T., and Ekstrom, A.D. (2013). Frequency-specific network connectivity increases underlie accurate spatiotemporal memory retrieval. *Nat. Neurosci.* 16, 349–356.
- Cornwell, B.R., Johnson, L.L., Holroyd, T., Carver, F.W., and Grillon, C. (2008). Human hippocampal and parahippocampal theta during goal-directed spatial navigation predicts performance on a virtual Morris water maze. *J. Neurosci.* 28, 5983–5990.
- Guitart-Masip, M., Barnes, G.R., Horner, A., Bauer, M., Dolan, R.J., and Duzel, E. (2013). Synchronization of medial temporal lobe and prefrontal rhythms in human decision making. *J. Neurosci.* 33, 442–451.
- Kaplan, R., Bush, D., Bonnefond, M., Bandettini, P.A., Barnes, G.R., Doeller, C.F., and Burgess, N. (2014). Medial prefrontal theta phase coupling during spatial memory retrieval. *Hippocampus* 24, 656–665.
- Staudigl, T., and Hanslmayr, S. (2013). Theta oscillations at encoding mediate the context-dependent nature of human episodic memory. *Curr. Biol.* 23, 1101–1106.
- Dalal, S.S., Jerbi, K., Bertrand, O., Adam, C., Ducorps, A., Schwartz, D., Martinerie, J., and Lachaux, J. (2013). Simultaneous MEG-intracranial EEG: New insights into the ability of MEG to capture oscillatory modulations in the neocortex and the hippocampus. *Epilepsy Behav.* 28, 283–302.
- Brincat, S.L., and Miller, E.K. (2015). Frequency-specific hippocampal-prefrontal interactions during associative learning. *Nat. Neurosci.* 18, 576–581.
- Siapas, A.G., Lubenov, E.V., and Wilson, M.A. (2005). Prefrontal phase locking to hippocampal theta oscillations. *Neuron* 46, 141–151.
- Anderson, K.L., Rajagovindan, R., Ghacibeh, G.A., Meador, K.J., and Ding, M. (2010). Theta oscillations mediate interaction between prefrontal cortex and medial temporal lobe in human memory. *Cereb. Cortex* 20, 1604–1612.
- Fell, J., and Axmacher, N. (2011). The role of phase synchronization in memory processes. *Nat. Rev. Neurosci.* 12, 105–118.
- Hasselmo, M.E., Bodelón, C., and Wyble, B.P. (2002). A proposed function for hippocampal theta rhythm: separate phases of encoding and retrieval enhance reversal of prior learning. *Neural Comput.* 14, 793–817.
- Ranganath, C., and Paller, K.A. (1999). Frontal brain potentials during recognition are modulated by requirements to retrieve perceptual detail. *Neuron* 22, 605–613.
- Buzsáki, G. (2002). Theta oscillations in the hippocampus. *Neuron* 33, 325–340.
- Jezeq, K., Henriksen, E.J., Treves, A., Moser, E.I., and Moser, M.B. (2011). Theta-paced flickering between place-cell maps in the hippocampus. *Nature* 478, 246–249.
- Capocchi, G., Zampolini, M., and Larson, J. (1992). Theta burst stimulation is optimal for induction of LTP at both apical and basal dendritic synapses on hippocampal CA1 neurons. *Brain Res.* 597, 332–336.
- Sederberg, P.B., Kahana, M.J., Howard, M.W., Donner, E.J., and Madsen, J.R. (2003). Theta and gamma oscillations during encoding predict subsequent recall. *J. Neurosci.* 23, 10809–10814.

32. Long, N.M., Burke, J.F., and Kahana, M.J. (2014). Subsequent memory effect in intracranial and scalp EEG. *Neuroimage* 84, 488–494.
33. Addante, R.J., Watrous, A.J., Yonelinas, A.P., Ekstrom, A.D., and Ranganath, C. (2011). Prestimulus theta activity predicts correct source memory retrieval. *Proc. Natl. Acad. Sci. USA* 108, 10702–10707.
34. Hanslmayr, S., and Staudigl, T. (2014). How brain oscillations form memories—a processing based perspective on oscillatory subsequent memory effects. *Neuroimage* 85, 648–655.
35. Oehrn, C.R., Baumann, C., Fell, J., Lee, H., Kessler, H., Habel, U., Hanslmayr, S., and Axmacher, N. (2015). Human hippocampal dynamics during response conflict. *Curr. Biol.* 25, 2307–2313.
36. Simons, J.S., and Spiers, H.J. (2003). Prefrontal and medial temporal lobe interactions in long-term memory. *Nat. Rev. Neurosci.* 4, 637–648.
37. Canolty, R.T., Edwards, E., Dalal, S.S., Soltani, M., Nagarajan, S.S., Kirsch, H.E., Berger, M.S., Barbaro, N.M., and Knight, R.T. (2006). High gamma power is phase-locked to theta oscillations in human neocortex. *Science* 313, 1626–1628.
38. Jay, T.M., and Witter, M.P. (1991). Distribution of hippocampal CA1 and subicular efferents in the prefrontal cortex of the rat studied by means of anterograde transport of Phaseolus vulgaris-leucoagglutinin. *J. Comp. Neurol.* 313, 574–586.
39. Xu, W., and Südhof, T.C. (2013). A neural circuit for memory specificity and generalization. *Science* 339, 1290–1295.
40. Rajasethupathy, P., Sankaran, S., Marshel, J.H., Kim, C.K., Ferenczi, E., Lee, S.Y., Berndt, A., Ramakrishnan, C., Jaffe, A., Lo, M., et al. (2015). Projections from neocortex mediate top-down control of memory retrieval. *Nature* 526, 653–659.
41. Cohen, M.X. (2011). Hippocampal-prefrontal connectivity predicts mid-frontal oscillations and long-term memory performance. *Curr. Biol.* 21, 1900–1905.
42. Monaco, J.D., Knierim, J.J., and Zhang, K. (2011). Sensory feedback, error correction, and remapping in a multiple oscillator model of place-cell activity. *Front. Comput. Neurosci.* 5, 39.
43. Jones, M.W., and Wilson, M.A. (2005). Phase precession of medial prefrontal cortical activity relative to the hippocampal theta rhythm. *Hippocampus* 15, 867–873.
44. Kumaran, D., and McClelland, J.L. (2012). Generalization through the recurrent interaction of episodic memories: a model of the hippocampal system. *Psychol. Rev.* 119, 573–616.
45. Jo, Y.S., Park, E.H., Kim, I.H., Park, S.K., Kim, H., Kim, H.T., and Choi, J.S. (2007). The medial prefrontal cortex is involved in spatial memory retrieval under partial-cue conditions. *J. Neurosci.* 27, 13567–13578.
46. Stokes, M.G., Kusunoki, M., Sigala, N., Nili, H., Gaffan, D., and Duncan, J. (2013). Dynamic coding for cognitive control in prefrontal cortex. *Neuron* 78, 364–375.
47. Tse, D., Langston, R.F., Takekama, M., Bethus, I., Spooner, P.A., Wood, E.R., Witter, M.P., and Morris, R.G. (2007). Schemas and memory consolidation. *Science* 316, 76–82.
48. Limpiti, T., Van Veen, B.D., and Wakai, R.T. (2006). Cortical patch basis model for spatially extended neural activity. *IEEE Trans. Biomed. Eng.* 53, 1740–1754.
49. Nolte, G. (2003). The magnetic lead field theorem in the quasi-static approximation and its use for magnetoencephalography forward calculation in realistic volume conductors. *Phys. Med. Biol.* 48, 3637–3652.
50. Gross, J., Kujala, J., Hamalainen, M., Timmermann, L., Schnitzler, A., and Salmelin, R. (2001). Dynamic imaging of coherent sources: Studying neural interactions in the human brain. *Proc. Natl. Acad. Sci. USA* 98, 694–699.